

Orbits of Globular Clusters in the Outer Galaxy: NGC 7006

Dana I. Dinescu^{1,2}, Steven R. Majewski^{1,3}, Terrence M. Girard⁴ and Kyle M. Cudworth⁵

ABSTRACT

We present a proper motion study of the distant globular cluster NGC 7006 based on the measurement of 25 photographic plates spanning a 40-year interval.

The absolute proper motion determined with respect to extragalactic objects is $(\mu_\alpha \cos \delta, \mu_\delta) = (-0.96, -1.14) \pm (0.35, 0.40)$ mas yr⁻¹. The total space velocity of NGC 7006 in a Galactocentric rest frame is 279 km s⁻¹, placing the cluster on one of the most energetic orbits ($R_a = 102$ kpc) known to date for clusters within 40-kpc from the Galactic center.

We compare the orbits — as determined from full space velocities — of four clusters that have apocentric radii larger than 80 kpc with those of Galactic satellites with well-measured proper motions. These clusters are NGC 5466, NGC 6934, NGC 7006 and Pal 13 and the satellites are the Sagittarius dwarf spheroidal galaxy (dSph), the Large Magellanic Cloud, Ursa Minor dSph and Sculptor dSph. Only NGC 5466 and NGC 6934 seem to have similar orbital parameters, indicating a possible phase-space association. NGC 7006, Pal 13 and the “pair” NGC 5466, NGC 6934 do not show any dynamical association with the Galactic satellites considered here. NGC 5466, NGC 6934, NGC 7006 and Pal 13 have orbits which are highly eccentric and of various inclinations with respect to the Galactic plane. In contrast, the orbits of the Galactic satellites are of low to moderate eccentricity and highly inclined. Based on orbit types, chemical abundances and cluster parameters, we discuss the properties of the hypothetical host systems of the remote globulars in the Searle-Zinn paradigm. It is apparent that clusters such as NGC 5466, NGC 6934 and NGC

¹Department of Astronomy, University of Virginia, Charlottesville, VA 22903-0818 (dd7a@virginia.edu, srm4n@virginia.edu)

²Astronomical Institute of the Romanian Academy, Str. Cutitul de Argint 5, RO-75212, Bucharest 28, Romania

³David and Lucile Packard Foundation Fellow, Cottrell Scholar of the Research Corporation

⁴Astronomy Department, Yale University, P.O. Box 208101, New Haven, CT 06520-8101 (girard@astro.yale.edu)

⁵Yerkes Observatory, 373 W. Geneva St. Williams Bay, WI 53191-0258 (kmc@yerkes.uchicago.edu)

7006 formed in systems that more likely resemble the Fornax dSph, rather than the Sagittarius dSph.

We also discuss plausible causes for the difference found so far between the orbit type of outer halo clusters and that of Galactic satellites and for the tentative, yet suggestive phase-space scatter found among outer halo clusters.

Subject headings: (Galaxy:) globular clusters: individual (NGC 7006) — Galaxy: kinematics and dynamics — astrometry — — galaxies: dwarf galaxies: individual (Large Magellanic Cloud, Fornax, Sagittarius, Ursa Minor, Sculptor)

1. Introduction

Since the early study of Sandage & Wildey (1967), NGC 7006 (C2059+160, $l = 63^\circ 8$, $b = -19^\circ 4$) has been known to be a globular cluster with an unusual red horizontal branch (HB) for its low metallicity ($[\text{Fe}/\text{H}] = -1.63$, Harris 1996 ⁶, hereafter H96). As an archetypical “second-parameter” cluster, and residing in the outskirts of the Milky Way at ~ 37 kpc from the Galactic center (GC), NGC 7006 is of considerable interest for formation scenarios of the assembling of the Galactic halo. Specifically, its age can constrain timescales of the assembling process, while the shape of the orbit can bring some insights as to how this process proceeded. Progress in determining the age of NGC 7006 has already been made by Buonanno *et al.* (1991), hereafter B91. From the analysis of the main sequence turnoff, B91 find no evidence that NGC 7006 is significantly younger than the bulk of the globular clusters. We will come back to this issue in our Discussion Section.

NGC 7006 is located very close to the radius where the the globular-cluster spatial distribution is truncated ($R_{GC} \sim 40$ kpc; from H96 there are no clusters between 40 and 70 kpc and only 6 clusters beyond 70 kpc; see also Zinn 1988). Yet, indications are that it is not at apogalacticon, as evidenced by the cluster’s large radial velocity (-384 km s^{-1} H96). A cluster likely to have excursions into the remote regions of the Galaxy is of interest because it may be dynamically associated with some of the Galactic satellite galaxies. Possible dynamical associations of some remote clusters with satellites based on radial velocities and locations have been proposed and studied already (e.g., Lynden-Bell & Lynden-Bell 1995; Palma, Majewski & Johnston 2001). However, in order to quantify such an association reliably one needs tangential velocities; it is the purpose of the present

⁶<http://physun.physics.mcmaster.ca/Globular.html>

work to determine them for NGC 7006 with the plate collection that we have available for this cluster. This study continues a program (Majewski & Cudworth 1993) to derive proper motions of a number of distant globular clusters and dwarf spheroidals (dSph).

The paper is organized as follows: in Section 2 we describe the photographic photometry and astrometry, in Section 3 we determine the absolute proper motion based on extragalactic objects, in Section 4 we derive the orbit of NGC 7006, and in Section 5 we discuss the cluster’s orbit in relation to orbits of other clusters and satellites that have well-measured absolute proper motions. Finally, in Section 6 we summarize our results.

2. Observations and Measurements

The photographic plate material available for this study, as well as the reduction procedure are very similar to those used in our previous paper on the cluster Pal 12 (Dinescu *et al.* 2000, hereafter D2K). Therefore we refer the reader to that paper for a detailed description of the procedures used. Table 1 summarizes the collection of 25 plates used in this study: 10 were taken with the Las Campanas DuPont 2.5 m reflector (scale = $10''.92 \text{ mm}^{-1}$), 7 with the KPNO 4 m reflector (scale = $18''.60 \text{ mm}^{-1}$ UBK7 corrector), and 8 with the Hale 5 m reflector (scale = $11''.12 \text{ mm}^{-1}$). An input catalog containing 5696 objects was prepared from a full digitization of plate CD3062, which is one of the deepest, good-quality plates among the modern-epoch set (Table 1). The digitized area is a square of $26'$ (143 mm for the DuPont plate scale) on a side. The digitization was done with the University of Virginia PDS microdensitometer ($30\text{-}\mu\text{m}$ pixel size), and preliminary positions, object diameters and object classification were determined using the FOCAS software⁷ (Valdes 1982, 1993). Using this input catalog, all of the plates were measured in a fine-raster, object-by-object mode with the Yale PDS microdensitometer, using a $12.7\text{-}\mu\text{m}$ pixel size for the DuPont 2.5 m and Hale 5 m plates, and a $10\text{-}\mu\text{m}$ pixel size for the KPNO 4 m plates. The image positions, instrumental magnitudes and image parameters were determined using the Yale Image Centering routines (two-dimensional, bivariate Gaussian fit, Lee & van Altena 1983). Due to the thermal drift in the PDS during long scans, eight stars were repeatedly measured in order to monitor and correct for drifts in the measurement system. This correction includes terms for translation and rotation. The image-centering accuracy for well-measured, stellar objects ranges between 0.8 and $1.7 \mu\text{m}$, depending on the plate emulsion.

⁷[ftp://iraf/noao.edu/iraf/docs/focas/focasguide.ps](ftp://iraf.noao.edu/iraf/docs/focas/focasguide.ps)

2.1. Photographic Photometry

The photographic photometry was calibrated using sequences obtained from CCD BV photometry from B91, their field 2, that includes their best-quality CCD photometry, and photoelectric photometry from Sandage & Wildey (1967) to ensure a good calibration at the bright end ($V \leq 15.5$). We have compared the B91 CCD photometry with the photoelectric photometry from Sandage & Wildey (1967) using four stars that were measured in both studies. We have found an offset of 0.1 mags in V and 0.2 mags in B between the two studies. We have then applied these offsets to the Sandage & Wildey (1967) photometry, such that the calibrating photometry is now on the system of B91.

For the B band we have used only the modern-epoch plates (8 plates, see Table 1) taken with the DuPont 2.5 m reflector, while for the V band we have used 2 modern-epoch plates and 3 intermediate-epoch plates taken with the KPNO 4 m reflector. Each plate requires a separate calibration and that calibration is determined via cubic spline interpolation to a calibration sequence. The final calibrated magnitude for each star is determined from the average of the measurements from each plate and the error in the magnitude is given by the scatter of the measurements, after outliers have been eliminated. From this scatter, we obtain an error of 0.03 in B and 0.05 in V for stars brighter than $V = 19$. For fainter magnitudes, the errors increase rapidly. The $B - V$ color is obtained from the straight differences of the averaged B and V magnitudes. The formal error in the $B - V$ color is of the order of 0.06 mag for well-measured stars ($V \leq 19$). A direct comparison of the calibrated magnitudes with the standard ones gives somewhat larger errors in the magnitudes: 0.05 in B , 0.09 in V and ~ 0.12 in $B - V$. This is because the calibrating sequences are determined primarily from standards located in a region centered on the cluster, where crowding effects increase the errors in the instrumental photographic magnitudes.

The photometry determined here was used in our astrometric reduction described below (Section 2).

2.2. Astrometry

All plates were precorrected for distortion as modeled by Cudworth & Rees (1991) for the DuPont 2.5 m and Chiu (1976) for the KPNO 4 m and Hale 5 m. The DuPont 2.5 m plates were also precorrected for differential refraction since, for this telescope, the differential refraction correction is comparable with the distortion correction (see D2K). In what follows all the linear dimensions correspond to the DuPont plate scale (see Table 1).

Magnitude-dependent systematics were modeled from the residuals given by the cluster stars, where the preliminary list of cluster stars is defined by positions in the color-magnitude diagram (CMD) (see Guo *et al.* 1993, Dinescu *et al.* 1996). The plate transformation included polynomials of up to fourth-order terms and linear color terms. As in our previous paper (D2K), we found significant color terms for both the KPNO 4 m and Hale 5 m plates (up to $5 \mu\text{m mag}^{-1}$), with the largest terms in the y -coordinate (aligned with declination). Since the Hale 5 m plates have the largest systematics among our three sets of plates, and the image quality degrades rapidly with distance from the plate center (D2K, Siegel *et al.* 2001), we have firstly determined preliminary proper motions from the DuPont 2.5 m and the KPNO 4 m plates, using an iterative central-plate-overlap algorithm (see for instance Girard *et al.* 1989). Then, with these preliminary proper motions, we modeled the Hale 5 m plates, that were afterwards introduced into the solution.

The proper motion is calculated for each star from a linear least squares fit of positions as a function of plate epoch. The error in the proper motion is given from the scatter about this best-fit line. Measurements that differ by more than $0''.2$ ($18 \mu\text{m}$) from the best-fit line were excluded.

In Figure 1, top panels, we show the proper-motion error in each coordinate as a function of magnitude for stars that had at least six measurements and that reside within a $14''.6$ box centered on the plate center. Outside of this box, the Hale 5 m measurements degrade quickly and objects tend to have measurements only from the two more modern set of plates. Well-measured stars ($16 < V < 18$) have a mean internal proper-motion error of 0.15 mas yr^{-1} in each coordinate. For these stars, the mean internal positional error at the mean epoch of 1977.0 is 2.7 mas ($0.25 \mu\text{m}$) in each coordinate. The middle panels show the the proper motions as a function of V magnitude, while the bottom panels show the proper motions as a function of $B - V$ color. We have highlighted the cluster stars as defined by the CMD of B91. A larger scatter is present in the y coordinate, which is mainly due to residual color terms in this direction. However, within the uncertainties, there are no significant magnitude and color trends in the proper motions over the range (Fig.1) defined by cluster stars.

The present study is complete only to $V \sim 19$ due to the shorter exposure times for this plate collection compared to that for the study of Pal 12 (D2K). Proper motion membership probabilities were also calculated, and they will be presented elsewhere.

3. Absolute Proper Motion

3.1. The Relative Motion of the Galaxies

We have identified the galaxies to be used as references for the absolute proper motion based on the distribution of image parameters such as peak density versus radius and instrumental magnitude. The image parameters for this selection are those derived from the KPNO 4 m plate 2874 (Table 1), which has a fine-grained emulsion. Each potential galaxy thus selected was visually inspected to ensure that blended and other spurious objects are not included in the list. Twenty six galaxies were so identified and, from these, we discarded those that had magnitudes and colors far outside the range of the cluster stars (Fig. 1). We were left with 19 galaxies, spread across the entire area measured (a square of 25' on a side). In addition, one known QSO resides in the field of NGC 7006: QSO2059+1604 (Harris *et al.* 1992).

As in our previous paper (D2K), position-dependent systematics are present in the proper motions as the distance from the plate center increases. These systematics are left because of our inability to determine a plate model accurately in the outer regions of the field, where both distortion and coma increase considerably for the Hale 5 m plates. Siegel *et al.* (2001) in their photographically similar study of Pal 13, restricted the usable area for astrometry to a circle of 5.5 radius (30 mm). Within this area they had 16 extragalactic objects. Unfortunately, the NGC 7006 field has only four extragalactic objects within a 30-mm radius from the plate center. Since galaxies have a poorer centering accuracy than do stars, due to their more shallow sloping profiles, the use of only four galaxies would not provide a suitably accurate calibration of the correction needed to yield an absolute proper motion.

In order to be able to use all 20 of the extragalactic objects, we apply the local-solution method developed in D2K and Dinescu *et al.* (1997). For each galaxy a local reference system is defined and the proper motion of the galaxy is re-determined with respect to this local system. The assumption is that, locally, both the galaxy and its reference system are affected by the same amount of geometric systematics and, thus, when referring one to the other, the systematics cancel out. The local reference system is chosen from field stars in a given magnitude range. The number of reference stars within a local system is chosen such that the area occupied is small enough that geometric systematics are unimportant and large enough that the sample size minimizes the scatter due to the intrinsic proper-motion dispersion of field stars in that particular magnitude range. For each local system, we have chosen 20 field stars with $16 < V < 19$; the radii of these local systems range between 0.7 and 1.5 (4-8 mm). The mean motion of this local reference system is defined by the median value of the proper motions and this value is subtracted from the motion of the galaxy. Details of this method are discussed at length in D2K. A slight modification from

D2K is the following. Since the galaxy does not necessarily reside in the center of mass of the local reference system, we apply a linear correction to account for this displacement, where the gradients in the proper motion in each coordinate are calculated from the proper motions of the local reference stars. We found that this method gives a more robust result than using a smaller number of local reference stars (e.g., seven) and applying directly the median given by these stars to the motion of the galaxy.

In Figure 2 we show the proper motions in each coordinate for the galaxies as a function of x , y and radius from the plate center. Proper motion units are mas yr^{-1} and throughout the panels we use the same scale for comparison purposes. The filled symbols of the first and third row of panels represent the proper motions as derived from the central plate-overlap method (Section 2.2), i.e., the global solution. The open symbols (the second and fourth row of panels) represent the proper motions as derived from the local solution. The error bars are the internal individual proper-motion errors as determined in Section 2.2. The larger error bars for galaxies situated at radii larger than 60 mm are due to the use of a shorter time baseline; these images were not measurable on the Hale plates. Clear trends with positions can be seen in the global solution and, consequently, we obtain the large scatter in the outer regions. Within a 40-mm radius we find an x proper-motion gradient of $\sim 0.05 \text{ mas yr}^{-1} \text{ mm}^{-1}$ and a y proper-motion gradient of $\sim 0.09 \text{ mas yr}^{-1} \text{ mm}^{-1}$ for the global solution. These gradients, over a distance of 20 mm, can easily produce a systematic shift of 1 to 2 mas yr^{-1} . For reference, the majority of the cluster stars are within a 20-mm radius. The local solution shows a significant improvement in terms of positional trends and scatter.

Assured that our galaxy proper motions are free of systematics we determine the mean correction to absolute proper motion — also called the zero point — as a weighted mean of the proper motions derived from the local solution. The weights are given by the individual proper-motion errors, (Section 2.2). The uncertainty in the zero point was calculated based on the scatter about the average and the weights.

Fig. 2 shows that galaxies that otherwise would cause a larger uncertainty in the solution are given an appropriately lower weight. In Figure 3 we also show the proper motions of galaxies as a function of magnitude and color. No significant trends are visible. The QSO is highlighted with a star symbol.

Our zero point with respect to field stars within $16 \leq V \leq 19$ is $\mu_{G,x}^F = 1.99 \pm 0.31 \text{ mas yr}^{-1}$ and $\mu_{G,y}^F = 4.83 \pm 0.37 \text{ mas yr}^{-1}$.

3.2. The Relative Mean Motion of the Cluster

The mean motion of the cluster is determined by fitting in each coordinate the sum of two Gaussians (that represent the cluster and the field) to the proper-motion distribution (e.g., Dinescu *et al.* 1996). Since proper-motion errors increase quickly with magnitude at the faint end (Fig. 1), we have restricted our sample to $16 \leq V \leq 20$. Also, due to position-dependent systematics discussed in the previous Section, we restrict the surveyed area for the relative motion of the cluster to a 3'.64 (20 mm) radius circle, centered on the plate center, which roughly coincides with the cluster center. Proper-motions larger than 15 mas yr⁻¹ in absolute value are also discarded from the proper-motion distribution to be modeled. In Figure 4 we present the observed, marginal proper-motion distributions (dotted line), smoothed by the individual proper-motion error (see details in Girard *et al.* 1989) for a total of 405 stars, together with the two-component Gaussian least-squares, best-fit model (solid line). In Table 2 we summarize all of the parameters from the best fit in each coordinate. The numbers in parentheses are formal estimates of the uncertainties as obtained from the fitting technique. The fitted parameters along each axis are: the number of cluster stars, the center and the dispersion of the cluster proper-motion distribution, and the center and the dispersion of the field proper-motion distribution. From these parameters, the ratio of cluster to field stars in the surveyed area is 1.55; in other words the cluster population dominates this area.

The mean relative cluster motion is taken to be the center of the cluster proper-motion distribution, and it is: $\mu_{C,x}^R = 0.28 \pm 0.03$ mas yr⁻¹ and $\mu_{C,y}^R = 0.34 \pm 0.05$ mas yr⁻¹. The uncertainty in the mean cluster proper motion is obtained by dividing the dispersion of the cluster distribution by the square root of the total number of cluster stars which is taken to be the average number from the x and y fit. This is a more realistic estimate of the uncertainty in the mean motion compared to that given by the formal estimate obtained from the fit (Table 2).

Cluster membership probabilities based on the proper motions were also determined using the method from Dinescu *et al.* (1996)⁸.

⁸A catalog of relative positions and proper motions, membership probabilities, and photographic photometry is available via e-mail, from the first author.

3.3. Final Absolute Proper Motion

The value of the cluster motion derived in the previous Section is with respect to a mean reference system comprised of mainly cluster stars but also field stars (the central-plate overlap or global solution described in Section 2.2). The reflex motion of the galaxies from the local solution is derived with respect to field stars in the magnitude range $16 \leq V \leq 19$. We must therefore accurately determine the (median) motion of this field-star component in our global-solution proper-motion system which is admittedly affected by position-dependent systematics.

To derive the field motion, with an adequate accuracy, requires the use of a larger number of field stars than what is available in the immediate vicinity of the cluster, i.e., the area over which the position-dependent systematics can be safely ignored. Thus, we include field stars up to 50 mm from the plate center and fit their proper motions as a function of radius using an even-term polynomial of fourth order, modeling out the systematic effects. The magnitude range of the sample is widened slightly, to $16 \leq V \leq 20$, to provide more stars. (The gradient with magnitude of the mean proper motion of the field is small enough to safely allow this.) More importantly, the sample has been cleaned of contamination by the cluster by eliminating all stars with proper motions within 1.4 mas yr^{-1} of the mean motion of the cluster. The radius of this circle was chosen to be $2 \times \max(\sigma_{C,x}, \sigma_{C,y})$. A further cut in x, y space, namely stars within 5 mm of the cluster, was also made to remove an overdensity that remained after the proper-motion cut. Finally, proper-motion outliers were discarded; those stars whose motions in either coordinate exceeded 20 mas yr^{-1} .

The field star sample, selected in this manner, consisted of approximately 1100 stars. The polynomial fits yielded a proper motion for the field, at the position of the cluster, of $\mu_{F,x}^R = -0.75 \pm 0.25 \text{ mas yr}^{-1}$, and $\mu_{F,y}^R = -3.35 \pm 0.24 \text{ mas yr}^{-1}$. The fourth-order fit provided a smooth representation of the median, as verified by overplotting the two. The standard error of the fits, in both the x and y components of μ_F^R , was 4.6 mas yr^{-1} .

A subtle correction must be applied to the uncertainties associated with this derived motion for the field. Approximately 400 of the field stars are the same as those used in the local solution for the galaxy motion, i.e., zero-point. Thus, only 700 of the 1100 stars in this field sample are drawn independently from the general field population of stars. The error associated with any offset between the average motion of the 400 stars in common and that of the general field population will exactly cancel out when $\mu_{F,x,y}^R$ is combined with $\mu_{G,x,y}^F$. The appropriate additional uncertainty associated with $\mu_{F,x,y}^R$, when it is being combined with $\mu_{G,x,y}^F$, is $700/1100$ of the formal values quoted above.

With this in mind, the absolute proper motion of NGC 7006 is $\mu_{C,x,y} =$

$\mu_{C,x,y}^R - \mu_{F,x,y}^R - \mu_{G,x,y}^F$. We obtain $\mu_{C,x} = -0.96 \pm 0.35$ mas yr⁻¹, and $\mu_{C,y} = -1.14 \pm 0.40$ mas yr⁻¹.

For comparison, had we used only two galaxies which are within a 4'-radius (22 mm) from the plate center, (the area that we believe is only negligibly affected by position-dependent systematics) and the global solution, we would have obtained the less accurate values of $\mu_{C,x} = -1.28 \pm 0.48$ mas yr⁻¹, and $\mu_{C,y} = -1.43 \pm 0.62$ mas yr⁻¹. We adopt the former values, based on the local solution above, as our best determination of the cluster's absolute motion.

4. The Orbit of NGC 7006

The standard solar motion with respect to the Local Standard of Rest (LSR) adopted here is $(U_{\odot}, V_{\odot}, W_{\odot}) = (-11.0, 14.0, 7.5)$ km s⁻¹ (Ratnatunga, Bahcall & Casertano 1989). The U component is positive outward from the GC. The adopted rotation velocity of the LSR is $\Theta_0 = 220.0$ km s⁻¹, and the solar circle radius is 8.0 kpc. The heliocentric distance to NGC 7006 is 40 ± 2 kpc (B91), and the heliocentric radial velocity is -384.1 ± 0.4 km s⁻¹; the Galactic coordinates are $l = 63^{\circ}77$, $b = -19^{\circ}41$ (H96). With the absolute proper motion derived in Section 3.3 we obtain the LSR velocity $(U, V, W) = (-116 \pm 62, -436 \pm 35, 149 \pm 60)$ km s⁻¹. The corresponding velocity in a cylindrical coordinate system centered on the GC is $(\Pi, \Theta, W) = (-179 \pm 41, 155 \pm 66, 147 \pm 66)$ km s⁻¹. In this left-handed system Π is positive outward from the Galactic rotation axis and Θ is positive in the direction of Galactic rotation, both as seen at the cluster. The local circular velocity has been removed, leaving these velocities in the Galactic rest frame.

With the initial position and velocity, we have integrated the orbit of NGC 7006 in a three-component, analytical model of the Galactic gravitational potential. The bulge is represented by a Plummer potential, the disk by a Miyamoto & Nagai (1975) potential, and the dark halo has a logarithmic form. For the exact form of the potential see Paczyński (1990).

The orbital elements were calculated as in Dinescu *et al.* (1999b) (hereafter DGvA99). They are averages over a 10-Gyr time interval. The uncertainties in the orbital elements were derived from the width of the distributions of orbital elements over repeated integrations with different initial positions and velocities. These positions and velocities were derived in a Monte Carlo fashion from the uncertainties in the observed quantities: proper motions, distance and radial velocity. We obtain an orbit of pericentric radius $R_p = 17 \pm 4$ kpc, apocentric radius $R_a = 102 \pm 28$ kpc, maximum distance above the

Galactic plane $z_{max} = 33 \pm 12$ kpc, eccentricity $e = 0.71 \pm 0.02$, and inclination with respect to the Galactic plane $\Psi = 26 \pm 9$ deg. The azimuthal period is $P_\varphi = (2.1 \pm 0.6) \times 10^9$ yr. With the present location of NGC 7006 at a distance from the GC of ~ 37 kpc and a distance of 13 kpc below the Galactic plane, the cluster is presently moving toward the Galactic plane and toward the Galactic center.

5. Discussion

5.1. Orbit Types of Globular Clusters and Galactic Satellites

We proceed now to compare the orbital parameters of NGC 7006 with those of the other globular clusters and Galactic satellites with well-determined absolute proper motions. The data for globulars are from DGvA99 for the majority of the clusters, D2K for Pal 12, and Siegel *et al.* (2001) for Pal 13. From the DGvA99 sample of clusters we have not included in the present analysis Pal 3, a very sparse and distant cluster (82 kpc, H96) whose absolute proper-motion determination is a very challenging measurement. The preliminary result (Majewski & Cudworth 1993) is likely to be revised as a more extensive, improved study is underway (Cudworth, private communication). Also, we have used revised heliocentric distances for clusters from H96, rather than the distances used in DGvA99. Globular clusters considered here are all within 40 kpc of the GC.

The Galactic satellites included in this study are: the Large Magellanic Cloud (LMC) and the dwarf spheroidals Sagittarius (Sgr), Ursa Minor (UMi) and Sculptor (Scl). The proper motion for the LMC is an average of three studies: Jones, Klemola, & Lin (1994), Kroupa, Röser & Bastian (1994), and Kroupa & Bastian (1997). The adopted heliocentric distance to the LMC is 49 ± 5 kpc, and the heliocentric radial velocity is 270 ± 4 km s⁻¹ (e.g., Kroupa & Bastian 1997, Meatheringham *et al.* 1988). Two proper-motion determinations are presented for Sgr: the one derived by Irwin *et al.* (1996) from Schmidt plates (Sgr1), and the one derived by Ibata *et al.* (1998a) from HST WFPC2 frames (Sgr2), and quoted in Irwin (1998). For Scl we have used the proper motion from Schweitzer *et al.* (1995) ($(\mu_\alpha \cos \delta, \mu_\delta) = (0.72, -0.06) \pm (0.22, 0.25)$ mas yr⁻¹), and for UMi we used the proper-motion determination from Schweitzer *et al.* (2001) ($(\mu_\alpha \cos \delta, \mu_\delta) = (0.056, 0.078) \pm (0.078, 0.099)$ mas yr⁻¹). Positions, heliocentric distances and heliocentric radial velocities for the dSphs were taken from the compilation of Mateo (1998).

Orbital parameters were determined as in DGvA99, in the potential model from Section 4. The orbital elements for clusters of interest and satellites are summarized in Table 3. Uncertainties in the orbital parameters were also determined in a Monte-Carlo fashion

(DGvA99); however, we chose not to display them in the following Figure because of the large range in their values from the low-energy to the high-energy domain. This is mainly because of the uncertainty in the heliocentric distance, which was chosen to be 10% of the distance (see DGvA99). Hence, clusters at large distances will have large uncertainties in their velocities and thereof in the total energy and orbital angular momentum. Uncertainties in the orbital parameters should however be kept in mind when a dynamical association is considered. We have listed the uncertainties in the orbital energy and orbital angular momentum for the objects of interest in Table 3. These values are indicative of how susceptible to uncertainties the apparent phase-space associations are.

In Figure 5, top panel, we show the total angular momentum L as a function of the total orbital energy, E , for clusters that have $E > -10^5 \text{ km}^2 \text{ s}^{-2}$. L was calculated as an average over the entire integration time (10 Gyr); while it is not a strictly conserved quantity for the potential we have used, it does provide some physical insight for the orbits as it can be thought of as the third integral of motion. This is particularly applicable for high-energy orbits, where the potential becomes more spherical (see discussion in Binney & Tremaine 1987).

The Galactic satellites and clusters of interest are labeled. Clusters are represented with open squares, and satellites with filled triangles. The units for energy are $10^4 \text{ km}^2 \text{ s}^{-2}$ and for angular momentum are $10^4 \text{ kpc km s}^{-1}$. Among the clusters with measured absolute proper motions that are located within 40 kpc from the GC, NGC 7006 is the most energetic. The other three clusters that fall in the same category ($R_a > 80 \text{ kpc}$, Table 3) are NGC 5466, NGC 6934 and Pal 13. None of these four most energetic clusters seem to match the large total angular momentum of the satellites at the same value of total orbital energy.

In the middle panel we show the orbital eccentricity as a function of the total orbital energy, for the entire energy range as defined by all globular clusters and the four Galactic satellites. In the low-energy domain ($E < -10^5 \text{ km}^2 \text{ s}^{-2}$), the distribution of eccentricities is rather uniform, while at larger values of the orbital energy the orbits of the clusters are preferentially of higher eccentricity. At the upper limit of the orbital-energy domain, the clusters form a distinct population that has highly eccentric orbits as opposed to the Galactic satellites that have orbits with moderate eccentricities. From the inspection of Table 3, the four most energetic globulars have highly-eccentric orbits, with a large range in the inclination with respect to the Galactic plane (also called plunging orbits), while the Galactic satellites have more circular orbits that are highly-inclined (also called polar orbits). From the data available so far, the orbits of outer halo clusters seem to be fundamentally different from those of the Galactic satellites.

In order to inspect whether a possible dynamical association of NGC 7006 with other clusters and any of the Galactic satellites considered is apparent, we also plot the total orbital energy as a function of the orbital angular momentum, L_z , for $E > -10^5 \text{ km}^2 \text{ s}^{-2}$ in the bottom panel of Fig. 5. From this plot, and from the previous plots in Fig. 5, it is apparent that only NGC 5466 and NGC 6934 have similar orbital elements, while Pal 13 and NGC 7006 stand alone in the phase space. Also, none of the four clusters considered here show any association with the Galactic satellites considered, if similar values of the integrals of motion are taken as evidence for a dynamical association. The association of NGC 5466 with NGC 6934 seen here was not remarked upon in DGvA99, although the same values of the proper motions were used. This new finding is due to the new heliocentric distances from H96 used here. However, the changes in the orbital elements caused by the new heliocentric distances are smaller than the uncertainties in these elements as derived in DGvA99. Therefore, this association should be regarded as tentative because of the large uncertainties in the orbits (see also Table 3).

We have marked two other clusters in Fig. 5, Pal 12 and NGC 5024 (M 53). A special note is to be made regarding these clusters. They share about the same locus as Sgr in all three plots. This is a clear indication of a common origin (see also Palma *et al.* 2001). Pal 12’s case has been extensively analyzed in D2K, where strong evidence for tidal capture from Sgr was presented. As for NGC 5024 — from the plots presented above — exploring such a scenario may be a well-justified exercise. However, we do not consider such an exercise in this work for two reasons: first, it would require a lengthy analysis that is beyond the scope of this paper, and second, the reliability of the analysis would be undermined by the proper-motion determination, which has too large of an uncertainty for this purpose. NGC 5024 has an absolute proper-motion determination which is subject to errors of $\sim 1 \text{ mas yr}^{-1}$ in each coordinate, while the size of the proper-motion is a few tenths of mas yr^{-1} (Odenkirchen *et al.* 1997). At an 18-kpc distance (H96) changes of the order of 1 mas yr^{-1} can significantly alter the orbit. In addition, the calibration to absolute proper motion is not with respect to extragalactic objects, but to a few *Hipparcos* stars. Usually these stars are much brighter (6 magnitudes) than cluster stars, and magnitude-dependent systematics are a major concern in photographic proper-motion studies (e.g., Girard *et al.* 1998, Platais *et al.* 1998, Dinescu *et al.* 1999a). We strongly encourage a possibly new and/or improved absolute proper-motion determination for NGC 5024.

Another note is required in this discussion. The Draco dSph also has an absolute proper-motion determination (Scholz & Irwin 1994). The proper-motion uncertainty in each coordinate is of the order of half a mas yr^{-1} . For a distant object (80 kpc), such a determination makes the orbit interpretation very uncertain. If considered however, Draco would have a highly eccentric orbit in our infinite-mass potential; in a more realistic

potential it escapes the Galaxy. Similarly, the LMC has a recent absolute proper-motion determination based on QSOs and a short time-baseline (8 years, Anguita *et al.* 2000). This determination disagrees with the more traditional determinations in the sense that the orbit is a lot more energetic. If this motion is correct, the LMC would have a highly eccentric orbit or escape from the Galaxy, depending on the model adopted for the potential. Since we feel that these results need confirmation from other studies, we chose not to interpret them at this point.

Although there is still little complete kinematical data on outer halo globulars ($R_{GC} > 15$ kpc) and Galactic satellites, a picture emerges from what we know so far. If indeed outer clusters have formed in individual, isolated, relatively low-mass systems (often referred to as proto-Galactic fragments or building blocks) that later were assimilated by the Milky Way (Searle & Zinn 1978, Zinn 1993, van den Bergh 2000 and references therein), then it is apparent that the orbits of these systems are quite different from those of the present-day Galactic satellites. It may be that the character of the orbit played a major role in the likelihood of survival of the satellite. Orbits that take satellites well into the inner regions of the Galaxy have a higher chance to be destroyed because the local Galactic density becomes comparable to the central density of the satellite, a condition that initiates tidal disruption. Models of satellite disruption show that the most dramatic effects take place during pericentric passages, when satellites can lose as much as a third of their mass (e.g., Johnston *et al.* 1999, Helmi 2000). For realistic satellites and host galaxies (Helmi 2000, also Bassino *et al.* 1994) models show that orbits with pericenters smaller than 20 kpc are highly destructive, with dissolution timescales of 2-3 radial periods; for our cases, about 4-6 Gyr.

The satellites that are present today therefore can be thought of as the survivors of a system undergoing preferential destruction. The main factors that contributed to the destruction are orbit shape and satellite mass. For massive systems ($M \geq 10^{10} M_{\odot}$), dynamical friction plays a major role as the satellite loses orbital energy and spirals into the denser, inner region of the Galaxy and subsequently suffers destruction (e.g., Walker, Mihos & Hernquist 1996). One such case could very well be the Magellanic Clouds (MC). According to the Murai & Fujimoto (1980) model, the apocentric distance for the MC has decreased by 50% in the past 10^{10} yr, placing the Clouds at a starting maximum distance of ~ 200 kpc. However, present-day satellites are low-mass systems ($\sim 10^7 M_{\odot}$, Irwin & Hatzidimitriou 1995). Only Fornax dSph and Sgr are somewhat more massive; they are also the only dSphs known to have their own globular-cluster systems. If the hypothetical parent satellites of the clusters NGC 5466, NGC 6934 NGC 7006 and Pal 13 had similar masses to Sgr and Fornax (up to $10^9 M_{\odot}$), then dynamical friction played a negligible role (e.g., Ibata & Lewis 1998b), and therefore the destruction is entirely due to the initial orbit

shape.

5.2. Clues from Chemical Abundances

The mass of a satellite plays an important role in its nucleosynthetic history: more massive satellites are able to retain enriched gas from older generations of stars. Abundance patterns, and in particular $[\alpha/\text{Fe}]$ ratios, are powerful indicators of the particulars of the star formation environment. α elements are thought to be produced in type II supernovae, while type Ia supernovae produce mostly iron-peak elements (Wheeler *et al.* 1989). The traditional relationship of $[\alpha/\text{Fe}]$ upon $[\text{Fe}/\text{H}]$ has a constant value of about 0.4 for $-2.0 \leq [\text{Fe}/\text{H}] \leq -1.0$, and a gradual decline to 0.0 at $[\text{Fe}/\text{H}] = 0.0$. This is often interpreted as type II supernovae-dominated enrichment for $[\text{Fe}/\text{H}] < -1$, followed by a gradually increasing contribution from type Ia supernovae as $[\text{Fe}/\text{H}]$ increases. For example, Shetrone, Côté & Sargent (2001) find that Draco, Sextans and Ursa Minor dwarfs have lower α -enhancements than do the globular clusters NGC 5272 (M 3), NGC 6341 (M 92) and NGC 2419, and halo field stars for the same range in metallicity, $-3.0 < [\text{Fe}/\text{H}] < -1.2$ (see their Figure 4). Specifically, Shetrone, Côté & Sargent (2001) determine that the three dSph galaxies have $0.02 \leq [\alpha/\text{Fe}] \leq 0.13$ dex, while the three globulars have a mean of $[\alpha/\text{Fe}] = 0.29 \pm 0.06$ dex, and halo field stars have a mean of $[\alpha/\text{Fe}] = 0.28 \pm 0.02$. For NGC 7006, Kraft *et al.* (1998) find $[\alpha/\text{Fe}] \sim 0.3$ (see their Table 5). McCarthy & Nemeč (1997) — from the analysis of the anomalous Cepheid V19 in NGC 5466 — find that the α -ratio has a typical value for globular clusters, ~ 0.3 (see their Figure 11), while NGC 6934 and Pal 13 have no such determinations to our knowledge. Thus two of the four clusters of interest here match the abundance pattern of the majority of halo globulars (see also Carney 1996). The lower $[\alpha/\text{Fe}]$ ratios for the relatively metal poor dSphs implies that these systems either lacked massive ($M > 10 M_{\odot}$) stars, or were not able to retain ejecta from type II supernovae and thereby incorporate these ejecta in the following generations of stars. Therefore abundance patterns suggest that NGC 5466 and NGC 7006 could not have formed in environments of the type inferred for the low-mass dSphs Draco, Sextans and Ursa Minor. In Sgr, however, most metal poor stars ($[\text{Fe}/\text{H}] \sim -1.5$) have $[\alpha/\text{Fe}]$ similar to typical halo stars and globulars (Smecker-Hane & McWilliam 1999), while $[\alpha/\text{Fe}]$ for Fornax stars has not been determined to date. Therefore, the suggestion is that the hypothetical host Galactic satellites of clusters NGC 5466 and NGC 7006 are more massive than the lower mass (as opposed to the more massive dSphs Fornax and Sgr) present-day dSphs.

We have also seen (Section 5.1) that the orbits of NGC 5466 and NGC 7006 are fundamentally different (plunging as opposed to polar orbits) from those of the lower

mass dSphs Ursa Minor and Sculptor. Both chemical and dynamical arguments suggest that at least some of the lower-mass dSphs may have a different formation history than the hypothetical parent fragments in which the outer halo globulars have formed. One long-standing hypothesis is that some dSphs formed as tidal condensations during the dynamical interaction between our Galaxy and a massive satellite such as the LMC, for instance. This scenario, initially inspired by the spatial alignment of some dSphs along great circles that include a more massive satellite (Kunkel & Demers 1976, Lynden-Bell 1982, Majewski 1994), has recently gained more ground from a dynamical point of view. For instance, Ursa Minor’s motion (Schweitzer *et al.* 1997, their Figure 1, our Fig. 5 and Table 4) shows that the dSph is moving along the great circle that contains the MC system and in the same sense as the MC system. Olszewski (1998) points out however, that UMi is more metal poor than the LMC and has a predominantly blue HB as opposed to the red HB of the LMC. Thus abundance arguments do not necessarily favor the tidal condensation scenario of UMi.

We turn now to investigate whether the hypothetical parent Galactic satellites of NGC 5466, NGC 6934, NGC 7006 and Pal 13 could have resembled the more massive dSphs Sgr and Fornax by comparing the dSphs’ cluster systems with the clusters under discussion.

5.3. Comparison with Sgr and Fornax dSph Cluster Systems

In Table 4 we summarize the metallicity, horizontal branch (HB) type (B-V/B+V+R), absolute integrated magnitude M_V and concentration parameters for NGC 5466, NGC 6934, NGC 7006 and Pal 13, for the clusters associated with Sgr (Da Costa & Armandroff 1995, D2K), and for the Fornax clusters. The data for the Galactic and Sgr clusters are from H96, except for the concentration parameter for Pal 12 which is from Rosenberg *et al.* (1998). For the Fornax clusters, the metallicity and HB type are from Buonanno *et al.* (1998, 1999), while the concentration parameter and absolute integrated magnitude are from Webbink (1985).

All four clusters considered here are known to be second-parameter clusters (NGC 5466: Buonanno *et al.* 1985; NGC 6934: Brocato *et al.* 1996, NGC 7006: Sandage & Wildey 1967, B91; Pal 13: e.g., Borissova *et al.* 1997). Recent age determinations argue that NGC 5466, NGC 6943 and NGC 7006 are not younger than the bulk of the globulars (see Rosenberg *et al.* 1999 for NGC 5466, Piotto *et al.* 1999 for NGC 6934, and B91 for NGC 7006), while Pal 13’s case may be somewhat uncertain (Borissova *et al.* 1997). Moreover, from an abundance analysis of NGC 7006 giants, Kraft *et al.* (1998) find that these stars have modest amounts of interior mixing, as opposed to stars in traditional

clusters such as NGC 6752 and M13. Kraft *et al.* (1998) propose that this moderate amount of mixing may be responsible for the second parameter effect in this cluster as opposed to age. Another argument in favor of a canonical old age for NGC 7006 is the ratio of α elements, which is similar to that of traditional globular clusters (Kraft *et al.* 1998, Section 5.2). Three of the Sgr clusters, namely M54, Ter 8 and Arp 2 are also known to have ages coeval with the rest of the halo globulars (Sarajedini & Layden 2000); however these clusters have traditional blue HB types for their metallicities, i.e. they do not display the second parameter effect. The other two Sgr clusters with red HB types, Ter 7 and Pal 12 are metal richer ($[\text{Fe}/\text{H}] > -1$), and younger by a few Gyr compared to traditional halo clusters (for Ter 7 see Sarajedini & Layden 2000 and references therein, for Pal 12 see, e.g., Rosenberg *et al.* 1998). The five Fornax clusters are known to display the second parameter effect (e.g., Buonanno 1998 and references therein). Recent HST-based age determinations show that the ages of Fornax clusters are also coeval with those of halo globular clusters (Buonanno *et al.* 1998). One exception is the extreme second-parameter cluster #4, which has been determined to be significantly younger based on the HST-data analysis of the main sequence turnoff (Buonanno *et al.* 1999).

Considering now only the coeval-age clusters, a sample that also includes only clusters with $[\text{Fe}/\text{H}] < -1.5$, we can see that NGC 5466, NGC 6934 and NGC 7006 have redder HB types than the Sgr clusters, and are more massive and more concentrated than these latter ones (Table 4). One exception is M54, which is significantly more massive. M54 has often been suggested to be the nucleus of Sgr (e.g., Larson 1996) and can therefore be thought of as non-typical for the globular cluster population. However, NGC 5466, NGC 6934 and NGC 7006 have HB types, masses and concentrations that closely resemble those of the Fornax cluster system (Table 4) rather than those of the Sgr system.

For the sake of completeness, we have also looked at the properties of what now are known to be old globular clusters in the LMC. We refer the reader to the recent HST-based analysis of the CMDs of clusters in the LMC done by Olsen *et al.* (1998), and the discussion in their paper concerning ages and the references therein. From their Figure 17b, that shows the relationship between metallicity and HB type, we can state that our clusters in discussion, NGC 5466, NGC 6934 and NGC 7006, have HB types that are similar to those of the old LMC globular clusters, for the corresponding metallicities.

Thus, at least three of the most energetic halo clusters known to date have properties that resemble those of the cluster systems in Fornax and LMC rather than those of the Sgr cluster system. It is also apparent that the second parameter effect for clusters NGC 5466, NGC 6934 and NGC 7006, for four clusters in Fornax and possibly for some of those in the LMC, is owed primarily to something other than age, perhaps related to the environment

where the clusters formed.

5.4. Concluding Remarks

The following facts now appear to be secure for three of the most energetic clusters known to date: they are fairly massive, they formed in a type II supernovae-dominated environment (except for NGC 6934 that has no α -ratio determination to date), they have highly eccentric orbits that are unlike the known orbits of the present-day satellites, and they display the second parameter effect while having ages that are coeval with the ages of traditional, first-parameter clusters.

We suggest that it is unlikely that NGC 5466, NGC 6934 and NGC 7006 formed in very massive satellites of the LMC type based on the highly eccentric character of the orbit ($e \geq 0.7$, Table 3). The N-body simulations of Tormen *et al.* (1998) that model the survival of substructure in dark halos show that dynamical friction leads to some amount of orbital circularization. Therefore, had dynamical friction played a significant role in the history of the hypothetical parent Galactic satellites of NGC 5466 and NGC 7006, we would have expected moderate orbital eccentricities. In other words, the initial orbit of the satellite should have been altered by dynamical friction before the satellite was disrupted. According to the HB-type versus metallicity relation however, clusters NGC 5466, NGC 6934 and NGC 7006 fit within the properties of the old LMC globulars.

It is more plausible that clusters such as NGC 5466, NGC 6934 and NGC 7006 formed in satellites of the size of Sgr or Fornax that were completely destroyed by tides rather early, owing to penetrating orbits into the denser regions of the Galaxy (Tormen *et al.* 1998). It is not clear however why the cluster properties such as mass and HB type of NGC 5466, NGC 6934 and NGC 7006 better match those of the Fornax clusters, rather than those of Sgr clusters. Based on the arguments discussed, we identify the Fornax dSph as highly representative of the Searle-Zinn proto Galactic fragments. Fornax’s survival may very well be due to its non-radial orbit.

Lastly, we note that, except for NGC 5466 and NGC 6934 which show a plausible dynamical association, NGC 7006 and Pal 13, stand alone in the phase space (Fig. 5). Specifically, the large scatter in orbital angular momentum (Fig. 5, bottom panel) shown for the “pair” NGC 5466-NGC 6934, NGC 7006 and Pal 13 hints to a more chaotic assemblage of the Milky Way outer halo, rather than the assemblage from the disruption of only one or two massive satellites.

6. Summary

We have measured the absolute proper motion of NGC 7006 and determined its orbit in a realistic Galactic potential. Among the clusters with measured space velocities within 40 kpc from the GC, NGC 7006 is the most energetic.

We have compared the orbital characteristics of the clusters NGC 5466, NGC 6934, NGC 7006 and Pal 13 — which are the most energetic clusters known to date ($R_a > 80$ kpc, see Table 3) — with those of satellite galaxies with well-measured proper motions. We find no dynamical association of NGC 7006 with other clusters or Galactic satellites with well-measured, full space velocities. This is also true for Pal 13. Only NGC 5466 and NGC 6934 show a possible common origin, as inferred from the integrals of motion, but no association with the Galactic satellites considered here.

The common feature of the orbits of these four clusters is the “orbit type”: highly eccentric, with various inclinations with respect to the Galactic plane. This is in contrast with the orbits of the present-day Galactic satellites which are of high inclination and small to moderate eccentricity. We discuss possible causes for this difference, under the assumption that outer halo clusters were formed in independently-evolving, proto galactic systems that were later assimilated by the Milky Way. Specifically, one hypothesis we set forth is that proto galactic fragments on highly eccentric orbits that penetrated the denser regions of the Galaxy underwent dissolution rather early and quickly, leaving for the present day only those systems on moderate eccentricities. Another explanation for the orbit-type discrepancy between present-day Galactic satellites and outer halo clusters is that some of the low-mass dSphs may have formed as condensations from the tidal interaction between a larger system, such as the MC and the Galaxy (e.g., Ursa Minor). Such dSphs have orbits that preserve the orbit type of the interacting system, i.e. the MC system that has a polar orbit. Both these processes could have worked to produce the present Galactic outer halo and the Galactic satellite system. More kinematical data for outer halo clusters and Galactic satellites would certainly help understand the formation picture of the halo. It would be very instructive to learn whether the large scatter in the phase space, together with the plunging character of orbits, persists for the more remote halo clusters.

We have compared the properties of NGC 5466, NGC 6934, NGC 7006 and Pal 13 with those of the clusters associated with Sgr and Fornax dwarf. Based on masses, concentrations, and HB types we conclude that at least NGC 5466, NGC 6934 and NGC 7006 are more likely to have been produced in Fornax-like systems.

We thank Allan Sandage and the Observatories of the Carnegie Institution for loan of the Hale 5 m plates taken by himself and W. Baade. We are grateful to Bill Schoening for

providing us the KPNO 4 m plates. We also wish to thank Tad Pryor, a diligent referee, whose thoughtful comments helped us improve this final version of the paper.

This research was supported by NSF grant AST-97-02521.

REFERENCES

- Anguita, C., Loyola, P. & Pedreros, M. H. 2000, *AJ*, 120, 845
- Binney, J. & Tremaine, S. 1987, in “Galactic Dynamics”, edited by Princeton University Press, p. 119
- Borissova, J., Markov, H., & Spassova, N. 1992, *A&AS*121, 499
- Brocato, E, Buonanno, R, Malakhova, Y., & Piersimoni, A. M. 1996, *A&A*, 311, 778
- Buonanno, R., Fusi Peci, F., Cappellaro, E., Ortolani, S., Richtler, T., & Geyer, E. H. 1991, *AJ*, 103, 1005 (B91)
- Buonanno, R., Corsi, C. E., Zinn, R., Fusi Pecci, F., Hardy, E., & Suntzeff, N. B. 1998, *ApJ*, 501, L33
- Buonanno, R., Corsi, C. E., Castellani, M., Marconi, G., Fusi Pecci, F., & Zinn, R. 1999, *AJ*118, 1671
- Carney, B. W. 1996, *PASP*108, 900
- Chiu, L. -T. G. 1976, *PASP*, 88, 803
- Cudworth, K. M., & Rees, R. F. 1991, *PASP*, 103, 470
- Da Costa, G. S. & Armandroff, T. E. 1995, *AJ*, 109, 2533
- Dinescu, D. I., Girard, T. M., van Altena, W. F., Yang, T. -G. & Lee, Y. -W. 1996, *AJ*, 111, 1205
- Dinescu, D. I., Girard, T. M., van Altena, W. F., Méndez, R., & López, C. E. 1997, *AJ*, 114, 1014
- Dinescu, D. I., van Altena, W. F., Girard, T. M, & López, C. E. 1999a, *AJ*, 117, 277
- Dinescu, D. I., Girard, T. M., & van Altena, W. F. 1999b, *AJ*, 117, 1792 (DGvA99)
- Dinescu, D. I., Majewski, S. R., Girard, T. M., & Cudworth, K. M. 2000, *AJ*, 120, 1892 (D2K)
- Girard, T. M., Grundy, W., López, C. E., & van Altena 1989, *AJ*, 98, 227
- Girard, T. M., Platais, I., Kozhurina-Platais, V., van Altena, W. F., López, C. E. 1998, *AJ*, 115, 855

- Guo, X., Girard, T. M., van Altena, W. F., & López, C. E. 1993, *AJ*, 105, 2182
- Harris, W. E., 1996, *AJ*, 112, 1487
- Harris, H. C., Guetter, H. H., Pier, J. R., Ables, H. D., Monet, D. G., Foltz, C. B., Chaffee, F. H., Boyle, B. J., & Irwin, M. J. 1992, *AJ*, 104, 53
- Helmi, A. 2000, Ph. D. Thesis, Leiden University
- Ibata, R. A., Irwin, M. J. & Lewis, G. 1998a, in preparation
- Ibata, R. A., & Lewis, G. F. 1998b, *ApJ*, 500, 478
- Irwin, M. J., Ibata, R. Gilmore, G. Wyse, R., Suntzeff, N. 1996, *ASP Conf. Series*, Vol. 92, *Formation of The Galactic Halo —Inside and Out*, ed. H. Morrison & A. Sarajedini (San Francisco: ASP), 841
- Irwin, M. J. 1998, in *IAU Symposium 192 - “The Stellar Content of Local Group Galaxies”*, editors P. Whitelock and R. Cannon, p. 29
- Johnston, K. V., Majewski, S. R., Siegel, M. H., Reid, I. N., & Kunkel, W. E. 1999, *AJ*, 118, 1719
- Kraft, R. P., Sneden, C., Smith, G. H., Shetrone, M. D., & Fulbright, J. 1998, 115, 1500
- Kroupa, P., & Bastian, U. 1997, *New Astronomy*, 2, 77
- Kroupa, P., Röser, S. & Bastian, U. 1994, *MNRAS*, 266, 412.
- Kunkel, W. E., & Demers, S. 1976, *Roy. Green. Obs. Bull.* 182, 241
- Larson, R. B., 1996, in “*Formation of the Galactic Halo...Inside and Out*”, *ASP Conf. Ser.* 92, edited by H. Morrison and A. Sarajedini, p. 14
- Layden, A. C. & Sarajedini, A. 2000, *AJ*, 119, 1760
- Lee, J. -F., & van Altena, W. F. 1983, *AJ*, 88, 1683
- Lynden-Bell, D. 1982, *Observatory*, 102, 202
- Lynden-Bell, D. & Lynden-Bell, R. M. 1995, *MNRAS*, 275, 429
- Majewski, S. 1994, *ApJ*, 431, L17
- Majewski, S. R. & Cudworth, K. M. 1993, *PASP*, 105, 987
- Mateo, M. 1998, *ARA&A*, 36, 435
- McCarthy, J. K., & Nemeč, J. M. 1997, *ApJ*, 482, 203
- Meatheringham, S. J., Dopita, M. A., Ford, H. C. & Webster, B. L. 1988, *ApJ*, 327, 651
- Miyamoto, M. & Nagai, R. 1975, *PASJ*, 27, 533

- Olsen, K. A. G., Hodge, P. W., Olszewski, E. W., Schommer, R. A., Suntzeff, N. B., & Walker, A. 1998, MNRAS, 300, 665
- Olszewski, E. W. 1998, in “Galactic Halos”, ASP Conf. Series, edited by D. Zaritsky, p. 70
- Paczyński, B. 1990, ApJ, 348, 485
- Palma, C., Majewski, S. R., & Johnston, K. V. 2001, ApJ, submitted
- Piotto, G., Zoccali, M., King, I. R., Djorgovski, S. G., Sosin, C., Dorman, B., Rich, M. R., & Meylan, G. 1999, ApJ, 117, 264.
- Platais, I., Kozhurina-Platais, V., Girard, t. M., can Altena, W. F., López, C. E., Hanson, R. B., Klemola, A. R., Jones, B. F., MacGillivray, H. T., Yentis, D. J., Kovalevsky, J., & Lindgren, L. 1998, A&A, 331, 1119
- Ratnatunga, K. U., Bahcall, J. N., & Casertano, S. 1989, ApJ, 291, 260
- Rosenberg, A., Saviane, I. Pioto, G. & Held, E. V. 1998, A&A, 339, 61
- Rosenberg, A., Saviane, I. Piotto, G, & Aparicio, A. 1999, AJ, 118, 2306
- Sandage, A. & Wildey, R. 1967, ApJ, 150, 469
- Scholz, R & irwin, M. J., 1994, in IAU Symp. 161: Astrometry from Wide-Field Imaging, 161, p. 535
- Schweitzer, A. E., Cudworth, K. M., Majewski, S. R., & Suntzeff, N. B. 1995, AJ, 110, 2747
- Schweitzer, A. E., Cudworth, K. M., & Majewski, S. R. 1997, in “Proper Motions and Galactic Astronomy”, ASP Conf. Series Vol. 127, edited by R. M. Humphreys, p. 103
- Schweitzer, A. E., Cudworth, K. M., & Majewski, S. R. 2001, AJ(submitted)
- Searle, L. & Zinn, R. 1978, ApJ, 225, 375
- Shetrone, M. D., Côté, P., & Sargent, W. L. W. 2001, 548, 592
- Siegel, M. H., Majewski, S. R., Cudworth, K. M., & Takamiya, M. 2001, AJ, in press
- Smecker-Hane, T., & McWilliam, A. 1999, in “Spectrophotometric Dating of Stars and Galaxies” ASP Conf. Proc. vol. 192, ed. I. Hubeny, S. Heap and R. Cornett, p. 150
- Tormen, G., Diaferio, A., & Syer, D. 1998, MNRAS, 299, 728
- Valdes, F. 1982, in Instrumentation in Astronomy IV, S.P.I.E. Proceedings, Vol. 331, p. 465
- Valdes, F. 1993, FOCAS User’s Guide, NOAO document
- Walker, I. R., Mihos, J. C., & Hernquist, L. 1996, ApJ, 460, 121

- Webbink, R. F., 1985, in “Dynamics of Star Clusters”, IAU Symp. 113, edited by J. Goedman and P. Hut, p. 541
- Wheeler, J. C., Sneden, C., Truran, J. W. 1989, ARA&A, 27, 279
- Zinn, R. 1988, in “The Harlow-Shapley Symposium on Globular cluster Systems in Galaxies; Proceedings of the 126-th IAU Symposium” Dordrecht-Kluwer, p. 37
- Zinn, R. 1993, in “The Globular Cluster-Galaxy Connection”, ASP Conf. Series, vol. 48, edited by G. H. Smith & J. P. Brodie, p. 38.

Fig. 1.— Proper-motion errors and proper motions as a function of magnitude (top and middle panel), and proper motions as a function of color (bottom panel). Filled circles represent cluster stars selected based on the CMD from B91. Proper-motion units throughout all of the figures are mas yr^{-1} .

Fig. 2.— Proper motions of extragalactic objects as a function of x coordinate, y coordinate, and radius from the plate center. The central plate-overlap or global solution is represented with filled circles, while the local solution is represented with open circles (see text for the description of the proper-motion solutions).

Fig. 3.— Proper motions of extragalactic objects as a function of magnitude and color, from the local solution. The QSO is highlighted with a star symbol.

Fig. 4.— Proper-motion marginal distributions along μ_x and μ_y . The dotted curves indicate the observed distributions, while the solid curves show the least-squares, best-fit model to the observed distributions by the sum of two Gaussians, one representing the cluster, the other the field stars.

Fig. 5.— Angular momentum as a function of orbital energy (top panel), eccentricity as a function of orbital energy (middle panel), and orbital energy as a function of the z component of the angular momentum, L_z (bottom panel). Globular clusters are represented with open squares, while the Galactic satellites are represented with filled triangles. The clusters discussed in the text and the satellites are labeled. The units for energy are $10^4 \text{ km}^2 \text{ s}^{-2}$ and for angular momentum are $10^4 \text{ kpc km s}^{-1}$.

Table 1. Photographic Plates

Plate #	Date (dd.mm.yy)	H.A.	Exp. (minutes)	Emulsion+Filter
Las Campanas DuPont 2.5 m ($10''.92 \text{ mm}^{-1}$)				
CD3037	19.06.93	0.68	30	IIa-O GG385
CD3038	19.06.93	23.98	30	IIa-O GG385
CD3039	19.06.93	23.43	30	IIa-O GG385
CD3048	20.06.93	0.37	45	IIa-D GG495
CD3049	20.06.93	23.40	45	IIa-D GG495
CD3056	21.06.93	0.22	30	IIa-O GG385
CD3057	21.06.93	23.68	30	IIa-O GG385
CD3058	21.06.93	23.12	30	IIa-O GG385
CD3062	16.08.93	23.85	45	IIa-O GG385
CD3098	21.08.93	0.30	45	IIa-O GG385
KPNO 4 m ($18''.6 \text{ mm}^{-1}$)				
2874	27.08.78	0.88	40	IIIa-J GG385
3121	22.08.79	23.58	30	IIa-O GG385
3122	22.08.79	23.03	30	IIa-O GG385
3123	22.08.79	22.45	30	IIa-D GG495
3124	23.08.79	1.17	30	IIa-D GG495
3125	23.08.79	0.67	30	IIa-D GG495
3138	24.08.79	23.65	30	IIa-O GG385
Hale 5 m ($11''.12 \text{ mm}^{-1}$)				
PH808s	02.10.54	0.17	10	103a-O GG13
PH809s	02.10.54	23.87	10	103a-O GG13
PH824s	03.10.54	23.27	20	103a-D GG11
PH1258s	11.08.56	22.57	10	103a-D GG11
PH1261s	11.08.56	21.78	10	103a-D GG11
PH1292s	13.08.56	23.62	7	103a-D GG11
PH1295s	13.08.56	22.92	7	103a-D GG11
PH1296s	13.08.56	22.73	7	103a-D GG11

Table 2. Model Parameters

	N_C	μ_C	σ_C	μ_F	σ_F
			(mas yr ⁻¹)		
X:	243(3)	0.280(3)	0.464(4)	-0.757(10)	2.919(10)
Y:	249(3)	0.343(5)	0.682(6)	-2.168(13)	3.817(11)

Table 3. Orbital Elements

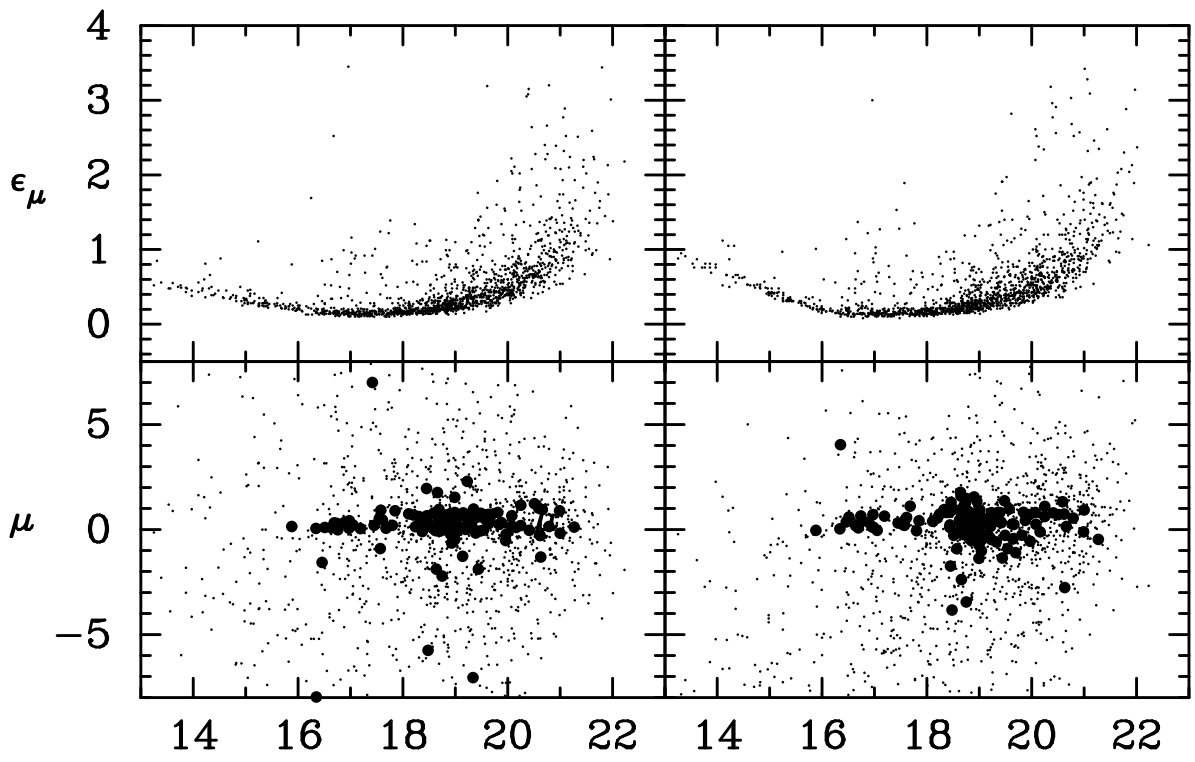
Object	E (10 ⁴ km ² s ⁻²)	L_z (kpc kms ⁻¹)	L	P_φ (10 ⁹ yr)	R_a (kpc)	R_p (kpc)	z_{max} (kpc)	e	Ψ (°)
NGC 5466	-2.4(1.6)	-610(287)	3715	2.0	96	9	54	0.84	37
NGC 6934	-2.6(1.9)	-54(623)	3766	1.9	88	9	56	0.81	73
NGC 7006	-2.0(0.9)	5420(1732)	6431	2.1	102	17	33	0.71	26
Pal 13	-2.3(0.8)	-3016(729)	4721	2.0	96	12	35	0.78	30
Scl	-0.7(1.4)	2038(606)	15858	3.0	124	61	91	0.34	69
LMC	-2.1(1.3)	2568(2405)	10820	2.0	85	41	60	0.35	67
UMi	-1.5(0.4)	3740(930)	13024	2.7	98	51	71	0.32	66
Sgr1	-4.5(0.8)	-108(233)	4357	1.1	50	13	31	0.58	58
Sgr2	-4.6(1.9)	827(986)	4294	1.0	48	13	29	0.56	57

Table 4. Cluster Parameters

Cluster	[Fe/H]	HB-type	M_V	c
NGC 5466	-2.22	0.58	-7.11	1.32
NGC 6934	-1.54	0.25	-7.65	1.53
NGC 7006	-1.63	-0.28	-7.68	1.42
Pal 13	-1.65	-0.20	-3.51	0.66
Sgr clusters				
M 54	-1.59	0.87	-10.01	1.84
Ter 7	-0.58	-1.00	-5.05	1.08
Arp 2	-1.76	0.86	-5.29	0.90
Ter 8	-2.00	1.00	-5.05	0.60
Pal 12	-0.94	-1.00	-4.48	1.08
Fornax clusters				
#1	-2.20	-0.20	-5.23	0.71
#2	-1.79	0.38	-7.30	1.08
#3 (NGC 1049)	-1.96	0.50	-8.19	1.83
#4	-1.90	-1.00	-7.23	1.82
#5	-2.20	0.44	-7.38	1.26

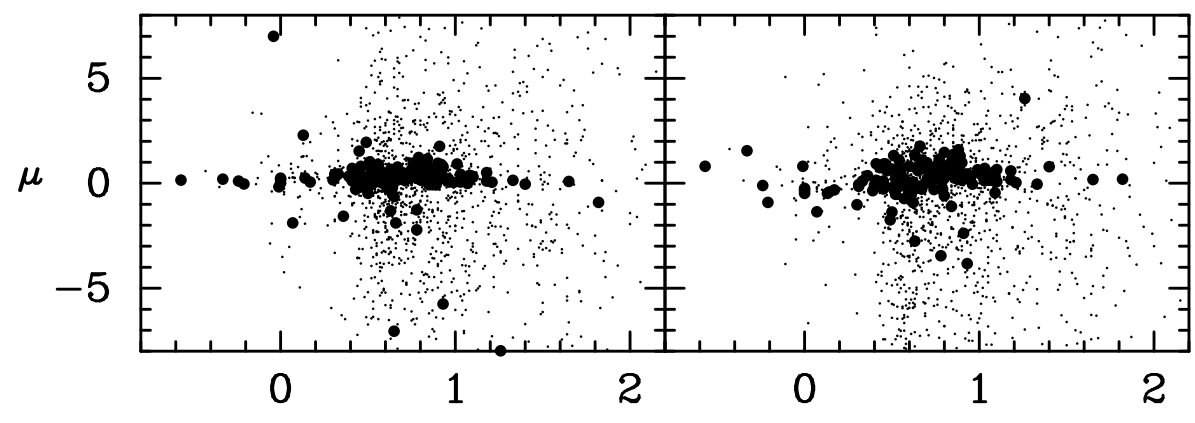
X

Y



V

V



B-V

B-V

